mixing ratio for H_2 equal to 1×10^{-8}, with an escape rate for H equal to 1×10^8 atom/cm^2-sec. Higher concentrations of O_2 would imply net conversion of H_2 and O_2 to H_2O and would require an additional source for O_2 of order 10^{15} g/year, which could in principle be supplied by photosynthesis followed by burial of organic material. We must note, however, that the photochemical steady state represented by model C is established exceedingly rapidly, on a time scale of less than 1 year. Photosynthesis with associated burial of organic carbon would cause a relatively slow rise in O_2. Model C indicates that the concentration of atmospheric H_2 should respond immediately to changes in O_2. Concentrations of OH and HO_2 are large, of order 10^8 and 10^9 cm^{-3}, respectively.

Nitrogen fixed by lightning in models A and C is rapidly converted to HNO_3 and is removed from the atmosphere by both dry and wet deposition, contributing ultimately to the reservoir of oceanic NO_3^-. The composition of fixed nitrogen in rain is dominated by HNO_3 as long as the mixing ratio for O_2 exceeds 10^{-11}. In model B, with the mixing ratio for O_2 equal to 2×10^{-12}, approximately 10 percent of the nitrogen fixed in lightning is converted to HNO_2. Even under these relatively extreme conditions, nitrate should be a significant end product. Indeed, source rates for nitrate as estimated here would imply that the primitive ocean could acquire an abundance of NO_3^- similar to that observed today on a time scale as short as 10^6 years (*11*). Under these circumstances one would not expect availability of fixed nitrogen to pose any serious limitation for the evolution of life on Earth (*12*).

The chemical processes discussed here suggest that the combination of lightning and subsequent photochemistry could result in steady removal from the atmosphere of soluble oxidized gases such as HNO_2 and HNO_3. There should be a corresponding source of reduced atmospheric species such as H_2. The almost inevitable segregation of reduced and oxidized compounds between atmosphere and ocean could have implications for the emergence of primitive biology and should be considered in more complete models for atmospheric evolution.

Y. L. YUNG
Division of Geological and Planetary Sciences, California Institute of Technology, Pasadena 91125
M. B. MCELROY
Center for Earth and Planetary Physics, Harvard University, Cambridge, Massachusetts 02138

References and Notes

1. C. C. Delwiche, *Chemistry in the Environment* (Freeman, San Francisco, 1973).
2. M. B. McElroy, in *Chemical Kinetics*, D. R. Herschbach, Ed. (Butterworth, London, 1976), p. 127.
3. G. Griffing, *J. Geophys. Res.* **82**, 943 (1977); J. F. Noxon, *ibid.* **83**, 3051 (1978); W. L. Chameides, D. H. Stedman, R. R. Dickerson, D. W. Rusch, R. J. Cicerone, *J. Atmos. Sci.* **34**, 143 (1977).
4. Y. B. Zel'dovitch and Y. P. Raizer, *Physics of Shock Waves and High-Temperature Hydrodynamic Phenomena* (Academic Press, New York, 1966); S. C. Lin, *J. Appl. Phys.* **25**, 54 (1954); G. Taylor, *Proc. R. Soc. London Ser. A* **201**, 159 (1950).
5. J. C. McConnell and M. B. McElroy, *J. Atmos. Sci.* **30**, 1465 (1973).
6. For thermodynamic calculations we used a computer code given by W. B. White, S. M. Johnson, and G. B. Dantzig [*J. Comput. Phys.* **28**, 751 (1958)]. Thermodynamic data were taken from *JANAF Thermodynamic Tables 1965* (PB-168370, Dow Chemical Co., Midland, Mich., 1965). In a typical calculation, we assumed a volume of air composed mainly of N_2, with about 2 percent H_2O and 0.03 percent CO_2. The equilibrium composition at 2500 K in terms of mixing ratios is calculated as: H, 1.5×10^{-3}; H_2, 3.4×10^{-3}; H_2O, 1.7×10^{-2}; N, 2.8×10^{-7}; NO, 1.7×10^{-3}; O, 4.2×10^{-4}; O_2, 8.4×10^{-4}; OH, 1.6×10^{-3}; CO, 1.9×10^{-4}; and CO_2, 1.5×10^{-4}.
7. Dissociation of NO occurs primarily in three bands around 1700 to 1900 Å. The diurnally averaged dissociation rates at zero optical depth for the $\delta(0,0)$, $\delta(1,0)$, and $\epsilon(2,0)$ bands are, respectively, 9.8×10^{-7}, 1.4×10^{-6}, and 3.1×10^{-7} sec^{-1}, adding up to a total dissociation rate of $J_6 = 2.7 \times 10^{-6}$ sec^{-1} [D. F. Strobel, *J. Geophys. Res.* **76**, 8384 (1971); private communication]. In calculating the effective yields of HNO_2 and HNO_3, we used the rain-out rates given by S. C. Wofsy, M. B. McElroy, and Y. L. Yung [*Geophys. Res. Lett.* **2**, 215 (1975)]. The results for models A, B, and C are, respectively, 100, 99.7, and 10 percent for removal of NO as HNO_2 and HNO_3.
8. We assume a thermal profile similar to that which applies today, except for the absence of an inversion in the stratosphere. The mixing ratio of H_2O is taken as 10 parts per million. Continuity equations are solved for all major species and we allow for transport of long-lived species such as H_2, CO_2, and H_2O. Conclusions are relatively insensitive to the choice of temperature profile and would be similar if we had used the profiles given by M. H. Hart [*Icarus* **33**, 23 (1978)]. A change in the temperature of the equatorial tropopause could alter the quantity of H_2O admitted to the upper atmosphere and might affect the rate of escape of hydrogen. The rate of hydrogen escape in models described here ranges from 10^8 to 10^{10} atom/cm^2-sec. This spread should adequately account for deficiencies in our understanding of thermal structure in the early atmosphere.
9. Note that the input of H_2 may be taken, for present purposes, as a measure of the net supply of reduced material. Other reduced gases, in particular CO, will be rapidly oxidized in the atmosphere with associated production of H_2, as discussed in (2).
10. These reactions take place preferentially under conditions where the concentration of H_2 is high relative to that of O. The reaction $N_2^+ + e \rightarrow N + N$ competes with reactions 11 when the mixing ratio for H_2 falls below 1×10^{-3}. The reaction $N_2^+ + O \rightarrow NO^+ + N$ dominates reactions 11 when $[O] \geqslant 0.1\ [H]$ (brackets denote concentration).
11. The oceans, at the current epoch, contain much less nitrate than one might anticipate on the basis of chemical equilibrium. In the absence of biological processes, lightning provides a path for the primitive atmosphere and hydrosphere to evolve toward a thermodynamically favored state. The rate of nitrate production represents a large flux of fixed nitrogen to the oceans but does not perturb the atmospheric nitrogen reservoir by more than a few percent over 10^9 years.
12. The role of nitrite and nitrate in the evolution of Precambrian organisms has been discussed by L. Margulis, J. C. G. Walker, and M. Rambler [*Nature (London)* **264**, 620 (1976)]. Influx of large quantities of HNO_2 and HNO_3 to the ocean could lower the mean *p*H and might cause an increase in the abundance of atmospheric CO_2 with possible implications for paleoclimate [L. T. Knauth and S. Epstein, *Geochim. Cosmochim. Acta* **40**, 1095 (1976)]. These matters are beyond the scope of this report. Our overall conclusions are unaffected by these complications. In particular, higher levels of CO_2 could provide additional paths for the lightning-related source of NO.
13. Rate constants are taken from Y. L. Yung and M. B. McElroy [*Icarus* **30**, 97 (1977)] and Y. L. Yung, D. F. Strobel, T. Y. Kong, and M. B. McElroy (*ibid.*, p. 26) and updated with information from Hudson (*14*).
14. R. D. Hudson, *NASA Ref. Publ. 1010* (1977).
15. We thank S. C. Wofsy for helpful discussions. Supported by NSF contract NSF-ATM-75-22723 to Harvard University and NASA grant NSG 7376 to the California Institute of Technology. Contribution 3109 of the Division of Geological and Planetary Sciences, California Institute of Technology.

4 August 1978; revised 13 November 1978

Observations of Hydrogen at Room Temperature (25°C) and High Pressure (to 500 Kilobars)

Abstract. *Hydrogen becomes a solid at 25°C when subjected to a pressure of 57 kilobars. The high-pressure phase appears as a transparent crystalline mass. The refractive index of the high-pressure phase increases sharply with pressure, indicating a density increase of similar magnitude. At 360 kilobars the calculated density of the high-pressure phase is 0.6 to 0.7 grams per cubic centimeter.*

When sufficient pressure is exerted on nitrogen or argon a liquid and then a solid appears even at room temperature. Thus, at some pressure one might expect hydrogen to solidify at room temperature. Furthermore, it has been suggested that all matter would become metallic under extreme pressure. Is it possible to make metallic hydrogen? Some theoretical studies (*1*) answer this question affirmatively. Many experimental difficulties must be overcome before observations can be made to test this hypothesis. First, there is the problem of containing a sufficient volume of hydrogen that must ultimately be brought to what, for hydrogen, is a relatively high density. Then one must be able to exert on the hydrogen enormous pressures that are accurately known. Finally, one must be able to observe the pressure effects directly or indirectly. In the present study, experiments were designed to seal liquefied hydrogen into a pressure cell at cryogenic temperatures and afterward remove the cell from the assembly and permit it to warm to room temperature. The sealing pressure was sufficient to prohibit escape of the compressed gas. At room temperature the hydrogen pressure could then be increased further for study.

The diamond-anvil, high-pressure cell was a logical choice for these experiments because of the relative ease with which gases, liquids, and solid phases are contained and because of the extremely high and accurately calibrated pressure range that can be sustained (2). The experimental concept was tested successfully with liquid nitrogen and liquid helium. The observations reported here were reproduced numerous times per run in four separate experimental assemblies.

Experimental. A specially designed massive version of the cell was constructed of maraging steel. Figure 1 shows a diagram of this cell, cut away to reveal details of the mechanism. The sample compartment located between the two diamonds cannot be seen in the diagram, but is essentially the same as the one used previously by Mao and Bell (2). This cell was operated at cryogenic temperatures during loading of the liquefied gas by advancing the piston (part 4) in the cylinder (part 3), using a remotely controlled mechanism. The cell was designed so that it could be placed in a lever assembly for operation at room temperature after the sample compartment was filled with liquefied gas. The lever-arm mechanism is required to apply greater force than is available with the remote-control mechanism alone.

Other parts of the apparatus include a gas-liquid filler tube (made of stainless steel or copper) and a close-fitting surrounding vessel made of brass. The procedure for loading the sample chamber with hydrogen was to lower the apparatus into a liquid helium cryostat, keeping a distance from the liquid helium, so that the temperature of the cell remained at 17 K. A measured volume of hydrogen gas (3) was pumped continuously into the cell as the apparatus was lowered into the cryostat. The hydrogen liquefied at the low temperatures and filled all the empty spaces, including the sample chamber. The brass surrounding vessel prohibited escape of the liquid and caught a small amount of overflow.

The piston was advanced to seal the cell and pressurize the liquid hydrogen sample at 10 to 60 kbar. The apparatus was then withdrawn from the cryostat, and the cell was removed from the remote-control mechanism where it warmed to room temperature while clamped by the lever-arm.

Observations. Small ruby crystals (10 to 20 μm in diameter) that had been placed in the sample chamber were used for pressure measurement with reference to the calibrated pressure shift of the fluorescent R_1 line (4). The hydrogen sample was viewed through one of the diamond windows by microscope. At approximately 57 kbar and 25°C, hydrogen was observed to solidify to a mass of transparent crystals.

Figure 2 is a photomicrograph of a closed-circuit television (CCTV) image of solid hydrogen crystals at the freezing point in the cell (5). A minor amount of liquid is present at the junctions and boundaries between the hexagonal-shaped crystals.

At 25°C and 57 kbar solidification was rapid, almost instantaneous, and reversible. Individual crystals, such as those shown in Fig. 2, rapidly merged into a single clear transparent solid with no visible grain boundaries. This solid remained unchanged visually as the pressure was increased until approximately 360 kbar, where a gradual visual change to a denser crystalline solid was observed.

Figure 3 is a CCTV time-lapse photomicrograph through one of the diamond windows at 57 kbar and 25°C. The dark

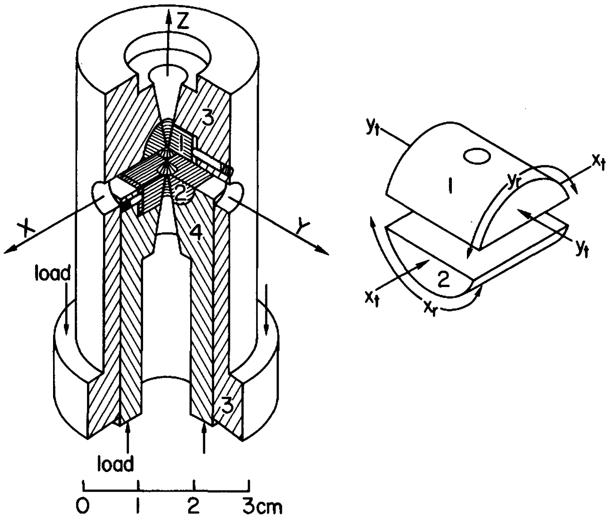

Fig. 1. Sketch of the diamond-anvil, high-pressure cell. The drawing on the right-hand side shows tungsten carbide pieces 1 and 2 in detail. Parts 3 and 4 are made of maraging steel.

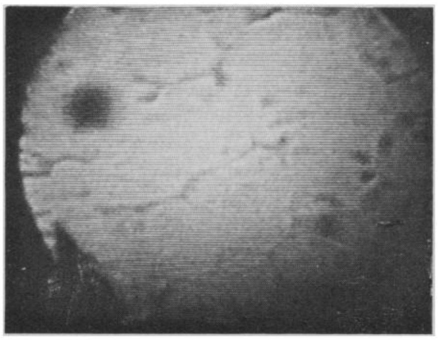

Fig. 2. Time-lapse closed-circuit television photomicrograph of hydrogen solidifying, taken through the diamond window (the circular image is 300 μm wide); the pressure was 57 kbar and the temperature 25°C. Dark defocused objects are dust particles on the outside of the diamonds. Note crystalline plates and their hexagonal triple-intersection boundaries. Liquid hydrogen exists along interfaces.

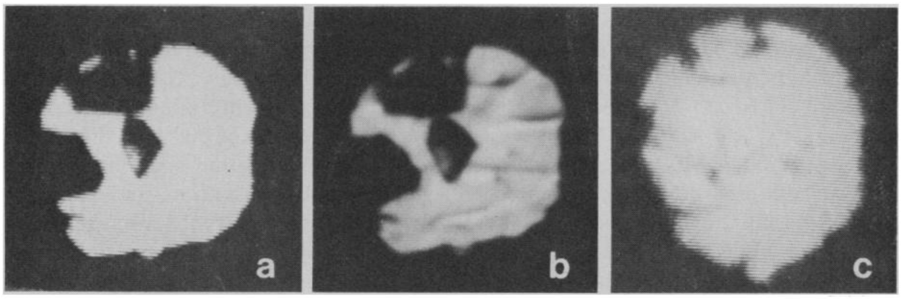

Fig. 3. Time-lapse closed-circuit television photomicrographs of solid hydrogen taken through the diamond window (field of view, 150 μm). (a) Dark ruby crystals in a clear transparent field of hydrogen fluid; 50 kbar and 25°C. (b) Formation of the high-pressure phase (gray) in equilibrium with the low-pressure fluid (light color); 57 kbar and 25°C. (c) High-pressure phase of hydrogen in contact with ruby at 300 kbar and 25°C; ruby crystals have almost disappeared as the refractive index of solid hydrogen approaches that of ruby.

objects (Fig. 3a) are ruby crystals, whose high relief is caused by their high refractive index relative to the surrounding hydrogen crystals. The gray-toned crystals (Fig. 3b) are the high-pressure phase, surrounded at the crystal margins with the light-colored, low-pressure liquid at this transition point. Relief along the boundaries is the Becke line, indicating that the high-pressure phase is considerably denser than the low-pressure phase.

As the pressure was increased above 57 kbar, the low-pressure phase disappeared, and the high-pressure phase became compressed and its refractive index increased. The ruby crystals became clear, and the visible boundary line between ruby and high-pressure hydrogen crystals disappeared at 360 kbar (Fig. 3c). Thus, the refractive indexes of the two materials had become the same. Accordingly, the results of calculations indicate that the density of the high-pressure hydrogen crystals had increased. The crystals were colorless at first, but they appeared to obtain a yellowish tint in some parts of the cell. A calculation of the specific gravity based on estimates of the average refractive index of this high-pressure phase gives 0.6 to 0.7 at 360 kbar. Between 360 and 500 kbar, no further changes were noted, except perhaps a slight darkening of the yellow color and a continuous increase in the index of refraction of the hydrogen phase relative to ruby.

The solidification is not observed to have the type of hysteresis associated with order-disorder transformations due to varying proportions of the ortho and para spin states of molecular hydrogen (*6*). Nevertheless, it is probable that both of these phases of hydrogen contain a mixture of states, possibly disordered.

Implications. The solidification point (57 kbar) observed at room temperature in this study is very close to that predicted (*7*). The room-temperature solid phase observed to 500 kbar in this study is not related to the known, complex, low-temperature structural transformations in hydrogen and does not appear to change at approximately 120 kbar, which was calculated for the transformation. (*6*).

The specific-gravity value of 0.6 to 0.7 for the high-pressure phase at 360 kbar agrees within the uncertainty with the values for generalized models of solid hydrogen calculated from theory by Liberman (*8*) and Ross and Shishkevish (*1*).

There is no direct evidence in the present experiments on which to base a choice of the physical process by which hydrogen will become (i) conducting in the molecular state or (ii) an atomic-like superconducting metal. A gradual, high order-type transition to the metallic state, similar to the metallic transition in iodine, could occur in hydrogen, and it has been stressed, for example, that measurements of electrical conductivity alone in high-pressure experiments with hydrogen are likely to be ambiguous (*1*).

The liquid and the new high-pressure phase of hydrogen are amenable to further characterization by measuring the Raman spectra, visible and near-infrared spectra, and electrical and magnetic properties. A separate set of experiments will be required for the generation of pressures on solid hydrogen above 500 kbar because of the nature of this technique (*2*). At present there is no reason to believe that pressures above 500 kbar on hydrogen cannot be achieved with the diamond-anvil, high-pressure apparatus.

H. K. MAO, P. M. BELL
Geophysical Laboratory,
Carnegie Institution of Washington,
Washington, D.C. 20008

References and Notes

1. A moderately complete review of theoretical models for the high-pressure behavior of hydrogen is given by M. Ross and C. Shishkevish, *Molecular and Metallic Hydrogen* (R-2056-ARPA, Rand Corporation, Santa Monica, Calif., 1977).
2. H. K. Mao and P. M. Bell, *Science* **200**, 1145 (1978).
3. The hydrogen gas used in these experiments was Linde ultrahigh purity grade (99.999 percent pure). It was piped by a liquid nitrogen trap through cleaned copper tubing with brass and stainless steel fittings. Evacuation cycles and continuous hydrogen purging (average rate, 0.5 liter/min) of the system were carried out repetitively up to the instant of filling the sample chamber. In the pressure cell, hydrogen was in contact with ruby, stainless steel, and diamond. No precipitates were observed on release of the pressure; the impurities in the hydrogen, therefore, were probably less than 0.01 percent. The ruby composition was laser grade Al_2O_3 plus 0.55 percent Cr by weight. Stainless steel was Ulbrich type 301, full hard, iron plus C (0.117 percent by weight), Mn (1.09), Si (0.49), P (0.026), S (0.011), Cr (16.93), Ni (7.35), Mo (0.31), Cu (0.23), and N (0.0370).
4. H. K. Mao, P. M. Bell, J. Shaner, D. Steinberg, *J. Appl. Phys.* **49**, 3276 (1978).
5. The image was recorded on a Panasonic time-lapse videotape recorder from a Hitachi CCTV unit.
6. R. L. Mills, *J. Low Temp. Phys.* **31**, 423 (1978).
7. D. H. Liebenberg, R. L. Mills, J. C. Bronson, *Phys. Rev. B* **18**, 4526 (1978).
8. D. A. Liberman, *Los Alamos Sci. Lab. Rep. LA-4727-MS* (1971).

30 January 1979

Mars Gravity: High-Resolution Results from Viking Orbiter 2

Abstract. *Doppler radio-tracking data have provided detailed measurements for a martian gravity map extending from 30°S to 65°N in latitude and through 360° of longitude. The feature resolution is approximately 500 kilometers, revealing a huge anomaly associated with Olympus Mons, a mascon in Isidis Planitia, and other anomalies correlated with volcanic structure. Olympus Mons has been modeled with a 600-kilometer surface disk having a mass of* 8.7×10^{21} *grams.*

On 25 October 1977, the periapsis altitude of the Viking Orbiter 2 spacecraft was lowered to 300 km. This event provided a unique opportunity for the acquisition of nearly global, detailed measurements of the martian gravity field. Earlier data had been acquired with the spacecraft at much higher altitudes where gravity effects were significantly attenuated and feature resolution was very limited. These analyses (*1–3*) revealed principally the regional Tharsis gravity high and flanking lows in the Chryse and Amazonis lowlands. Some investigators (*2*) determined the Hellas basin as a gravity low. Using a very limited set of data from Viking Orbiter 1 at a periapsis altitude of 300 km, Sjogren *et al.* (*4*) provided some corroborating results for Olympus Mons and Alba Patera; but the zone of maximum sensitivity is very narrow, and these results are overshadowed by the much greater detail and coverage of the Viking Orbiter 2 data.

The Viking Orbiter 2 data were obtained at a fortuitous time. A variety of problems had arisen in earlier observing periods: (i) the Earth-Mars distance was larger, and thus the return signals were weaker; (ii) the signal path was in closer proximity to the sun, and thus there was larger corruption by the solar plasma; (iii) occultation of the periapsis region occurred; and (iv) the periapsis altitude was larger. During the data collection from 25 October 1977 through March 1978, all of the above problems were eliminated and the line of sight from Earth was never more than 20° from the orbital plane of the spacecraft. This geometry allowed an almost direct measure of the vertical component of gravity; the periapsis altitude was between 270 to 300 km. The 80° orbital inclination of Viking 2 was another favorable factor, which made possible extensive coverage in latitude.

The requested tracking coverage was not obtained because of the many conflicting demands on the tracking station time. The resulting gaps in coverage are seen in Fig. 1, in which the near-vertical lines represent the locus of the spacecraft during the data taking. The Doppler signal was sampled every 10 seconds,

0036-8075/79/0309-1006$00.50/0